Catalysis Communications 43 (2014) 197–201

Contents lists available at ScienceDirect

Catalysis Communications

journal homepage: www.elsevier.com/locate/catcom

Short Communication

Efficient structured catalysts for ethylene production through the ODE reaction: Ni and Ni–Ce on ceramic foams

J.P. Bortolozzi, L.B. Gutierrez, M.A. Ulla *

Instituto de Investigaciones en Catálisis y Petroquímica, INCAPE (FIQ, UNL-CONICET), Santiago del Estero 2829, 3000 Santa Fe, Argentina

ARTICLE INFO

Article history:
Received 16 August 2013
Received in revised form 8 October 2013
Accepted 10 October 2013
Available online 17 October 2013

Keywords:
Nickel oxide
Nickel–cerium oxides
Ceramic foams
Oxidative dehydrogenation of ethane

ABSTRACT

Ni and Ni–Ce oxides alumina-supported formulations onto alpha-alumina foams were prepared, characterized and evaluated in the oxidative dehydrogenation of ethane (ODE) reaction. The catalysts were appropriately deposited on ceramic foams with a uniform, mechanically stable coverage. Besides, the structured systems were active and selective in the ODE reaction, demonstrating that the incorporation method was successful to obtain adequate active sites. Cerium markedly improved the ethane conversion due to a synergistic effect with nickel oxide, thus leading to a significant increment in ethylene productivity compared to that of the cerium-free system. An optimal Ce/Ni ratio was found which maximized the catalytic performance.

1. Introduction

Structured catalysts are generally constituted by a catalytic formulation deposited onto a substrate [1]. Different types of materials such as ceramic compounds and alloys are employed for manufacturing the substrates [2,3]; these materials, in turn, could conform different types of arrangements such as monoliths [4,5], meshes [6,7] or foams [8]. Ceramic foams have attracted attention as potential substrates for structured systems because they are characterized by high porosity and surface geometry/volume ratio and low weight [9–11]. Another significant feature is their enhanced radial thermal conductivity that could be useful for exothermal-type reactions such as partial oxidation or alkylation [12,13]. In addition, nearly isothermal behavior with minimal "hot spots" generation can be obtained with dense foams [14].

Significant scientific efforts focused on obtaining more efficient catalysts for ethylene production through the oxidative dehydrogenation of ethane (ODE) reaction have been published [15,16]. The first study to investigate powder catalysts based on *bulk* nickel–cerium oxides was an article published by Solsona et al. The addition of cerium to NiO induced significant changes in its catalytic performance, although these changes depend on the catalyst composition [16]. A multimetallic MoVTeNbO oxide can be counted among the most efficient powder catalysts reported so far, but it presents a complex preparation method [17]. The active and selective component corresponds to an orthorhombic phase (M1). Recently, Nguyen et al. [18] reported that the M1 phase could not be produced on a pre-oxidized SiC foam to form a structured catalyst, starting from a slurry which contains the precursors of a powder formulation. These authors reported that the layer formed not only contained the M1 phase but also another phase (M2), which was less active and selective. Therefore, the reproducibility of active phases present in a powder formulation to build a catalytically active, selective and technologically feasible structured system is still a major challenge.

Essakhi et al. and Bortolozzi et al. found that the use of structured systems could improve the ethane conversion [19,20] although the presence of foreign components from the substrate produces variations in the catalytic performance. This behavior can be modified by both the incorporation of a chemical barrier [19] and the reduction of the calcination temperature of the support deposited on the substrate [20].

Another alternative to avoid these harmful species is using materials that present chemical affinity with the catalytic formulation and prevent the migration process of the undesired components toward the catalytic film.

In this context, the goal of this contribution was to obtain catalytically active and selective Ni and Ni–Ce oxides alumina-supported formulations deposited onto α-alumina foams. After a detailed morphological and physicochemical characterization, the structured systems were evaluated in the ODE reaction.

2. Experimental

2.1. Preparation method

Pieces of α-Al_2O_3 foams (Goodfellow®, 65 ppi) were washed in deionized water and acetone for 60 min. Then, the support (colloidal γ-Al_2O_3, Nyacol® AL20DW) was deposited by vacuum-assisted immersion. Finally, they were calcined in air at 550 °C for 2 h.

For the incorporation of active metals, aqueous solutions (0.4 M) of Ni$(NO_3)_2.6H_2O$ and Ce$(NO_3)_3.6H_2O$ were used. The excess was removed by

* Corresponding author. Tel./fax: +54 342 4536861.
E-mail address: mulla@fiq.unl.edu.ar (M.A. Ulla).

1566-7367/$ – see front matter
http://dx.doi.org/10.1016/j.catcom.2013.10.011

blowing and then dried at 120 °C for 1 h. Finally, all systems were calcined in air at 550 °C for 4 h.

The structured catalysts were prepared in monometallic (Ni, Ce) and bimetallic (Ni–Ce) oxide forms with a total metal loading close to 15 wt.%. For bimetallic oxide forms, the precursor solutions were prepared with four atomic ratios of Ce/Ni = 0.05, 0.11, 0.17 and 0.25. The prepared systems were designated as NiCe (x) – AF, where x corresponds to the Ce/Ni nominal atomic ratio.

2.2. Catalyst characterization

Crystalline phases were identified by X-ray Diffraction (XRD). The analysis was performed in a range of 20–85° (1°/min) with a Shimadzu XD-D1 diffractometer.

Raman spectra were recorded using a LabRAM spectrometer (Horiba-Jobin-Yvon) with an Olympus confocal microscope (a 100× objective lens was used) equipped with a CCD detector (Laser power = 30 mW).

X-ray Photoelectron Spectroscopy (XPS) measurements were performed in a SPECS equipment with a hemispherical PHOIBOS 150 analyzer operating in the FAT mode. The spectra were obtained with a pass energy of 30 eV and Mg-Kα X-ray source power of 200 W. The peak fitting was performed with the CASAXPS software.

The mechanical stability of the catalytic coatings was analyzed with a TestLAB TB04 (40 kHz and 160 W) ultrasound equipment. The weight loss was determined after exposing the samples in acetone at RT for 1 h.

The morphology and distribution of the catalysts were characterized by Scanning Electron Microscopy (SEM) with a JEOL JSM 35C equipment with EDX energy-dispersive system operating at 20 kV.

2.3. Catalytic tests

The oxidative dehydrogenation of ethane was performed in a flow system operated between 300 and 450 °C. The feed composition was 6% O_2 and 6% C_2H_6 diluted in He.

The weight of the tested catalysts was ~0.3 g. The final flow was set to achieve a W/F ratio of 0.48 g s/cm^3. A second part of the experiments was conducted at fixed temperature (400 °C) with variable W/F ratio.

Reactants and products were quantified with a gas chromatograph (Shimadzu® GC 2014) equipped with a packed column (HayeSep D®).

3. Results and discussion

3.1. Catalytic performance

Fig. 1 shows the catalytic behavior of the structured catalysts. The cerium-free system presents a moderate ethane conversion whereas the cerium-promoted systems show much higher values. The presence of a tiny amount of cerium (i. e. Ce/Ni = 0.05) boosts the ethane conversion around 80% with respect to the monometallic oxide catalyst.

The conversion values at each temperature progressively increased while the cerium content of the catalyst increased, until the Ce/Ni ratio of 0.17 was reached being almost 40% at 450 °C, whereas the catalyst with a higher amount of Ce presented a lower conversion.

Fig. 2 depicts the ethylene selectivity with the ethane conversion increment at a fixed temperature. The cerium-free system shows high selectivity (~85%) at low conversion whereas a gradual decrease is observed when the conversion level rises. At 22% of conversion, the selectivity for Ni – AF catalyst reaches ~70%.

On the other hand, the samples promoted with cerium show lower selectivity than the monometallic oxide catalyst but they show the same trend with the increment in the ethane conversion. Even with a low amount of Ce, the cerium-promoted samples show lower selectivity than the cerium-free system for the same conversion. Hence, the promoter contributes to the direct oxidation of ethane to produce carbon oxides. Simultaneously, an increase in the Ce/Ni ratio provokes a faster decrease in selectivity. Therefore, the presence of cerium slightly favors the ethylene oxidation, too.

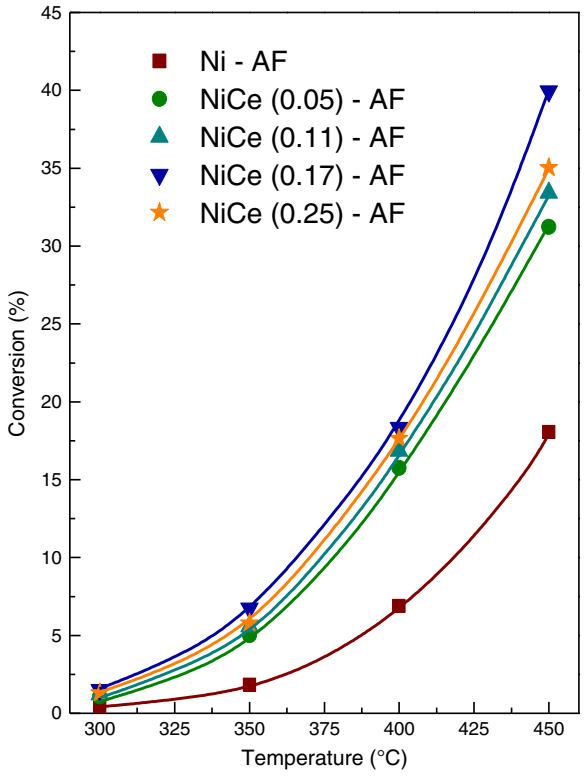

Fig. 1. Ethane conversion of the catalysts. Reaction conditions: W/F = 0.48 g s/cm^3, $C_2H_6/O_2 = 1$.

A nickel-free catalyst was also evaluated under the same reaction conditions. This system presented both low conversion and selectivity to ethylene, showing that cerium by itself is a non adequate active phase for the ODE reaction. Consequently, the active component is nickel oxide but the combination with cerium produces a beneficial effect that significantly enhances its catalytic performance.

It is noteworthy mentioning that oxygen conversion never reached 100% and no carbon monoxide was measured in the product stream in any catalytic test.

In order to evaluate the global catalytic behavior, Fig. 3 shows the ethylene productivity. In general, productivity improved with the addition of the promoter. The incorporation of cerium led to a marked increase of the global performance, mainly caused by the better conversion. The best productivity was achieved with the NiCe (0.17) –

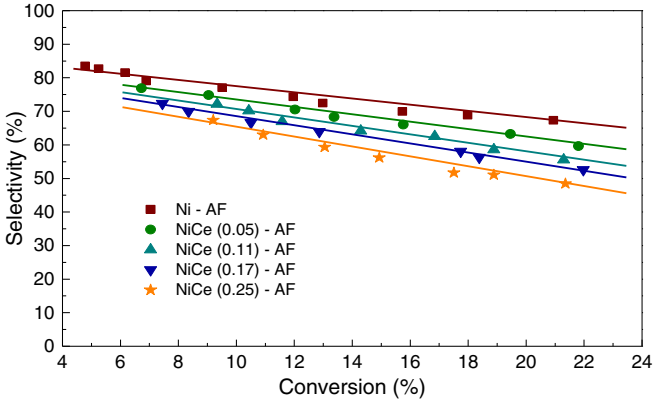

Fig. 2. Ethylene selectivity of the catalysts. Reaction conditions: T = 400 °C, W/F = variable, $C_2H_6/O_2 = 1$.

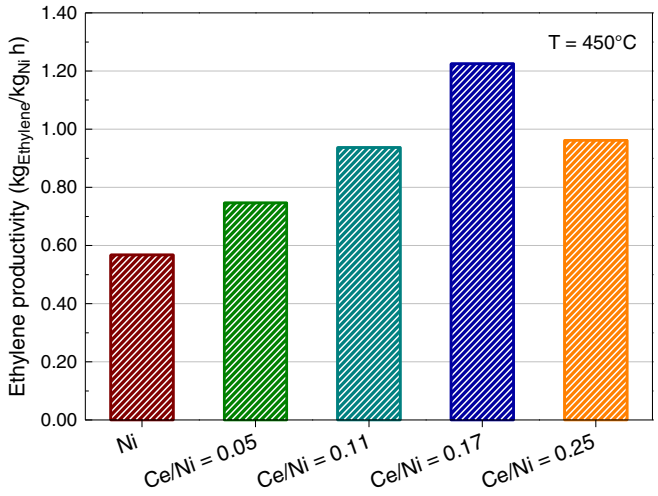

Fig. 3. Ethylene productivity of the catalysts. Reaction conditions: T = 450 °C, W/F = 0.48 g s/cm^3, C_2H_6/O_2 = 1.

AF system, reaching an increment of ~120% compared with the promoter-free catalyst.

All structured systems were tested during more than 20 h in reaction stream. After subsequent measurements, no significant modifications in either ethane conversion or selectivity to ethylene were found, thus demonstrating an acceptable stability.

3.2. Catalyst characterization

3.2.1. Morphology of the coatings

The walls of the ceramic foams present intrinsic roughness with irregular grains of sizes between 0.5 and 8 μm, approximately (Fig. 4.a and b). Therefore, it is unnecessary to modify the surface by treatments such as heating and/or chemical attack that generate imperfections to obtain an adequate anchorage of the deposited films.

After the immersions of the alumina foam into the support suspension and catalytic precursors, a relatively homogeneous and uniformly deposited film was obtained. The layer properly reproduced the substrate morphology along the ceramic structure. However, in certain sectors, some well defined cracks with an average thickness below 1 μm were observed (Fig. 4.c and d). It was also noted that micrometer sized pores on the surface remained, in general, not blocked (Fig. 4.c). The catalytic coating was not totally smooth and presented numerous nanometric rifts spread along the surface (Fig. 4.e).

3.2.2. Mechanical stability test

The mechanical stability of the films was examined by submitting the catalysts to an ultrasound treatment. All coatings deposited showed excellent adhesion which could be due to a strong physical and chemical compatibility between the substrate and the deposited catalytic layer. The weight loss percentage (relative to the total mass) was around ~1.0 wt.% after the total time of treatment. If the weight loss were referred to the coating mass, this value would rise up to ~6.0 wt.%, also demonstrating a high adherence.

The Ni – AF system showed the lowest adherence while the NiCe (0.25) – AF catalysts presented the highest. Although the differences were not significant, these results suggest that the catalyst composition affects adhesion to some extent.

3.2.3. Features of active phases

XRD patterns (not shown) of the structured systems showed the peaks corresponding to the substrate. These signals were very narrow revealing a high crystallinity degree of the alpha-alumina phase. The substrate diffraction pattern was consistent with that obtained in the literature (JCPDS 46-1212). However, the intensity peak ratios differed slightly which could be due to a preferential growth of crystals in the α-Al_2O_3 foam, resulting from the manufacturing process.

Additional signals could not be identified since the main peaks of NiO were overlapped with those of the α-Al_2O_3. Moreover, NiO could be highly dispersed and could form an amorphous phase onto the surface. Nevertheless, the NiCe (0.25) – AF pattern showed a broad

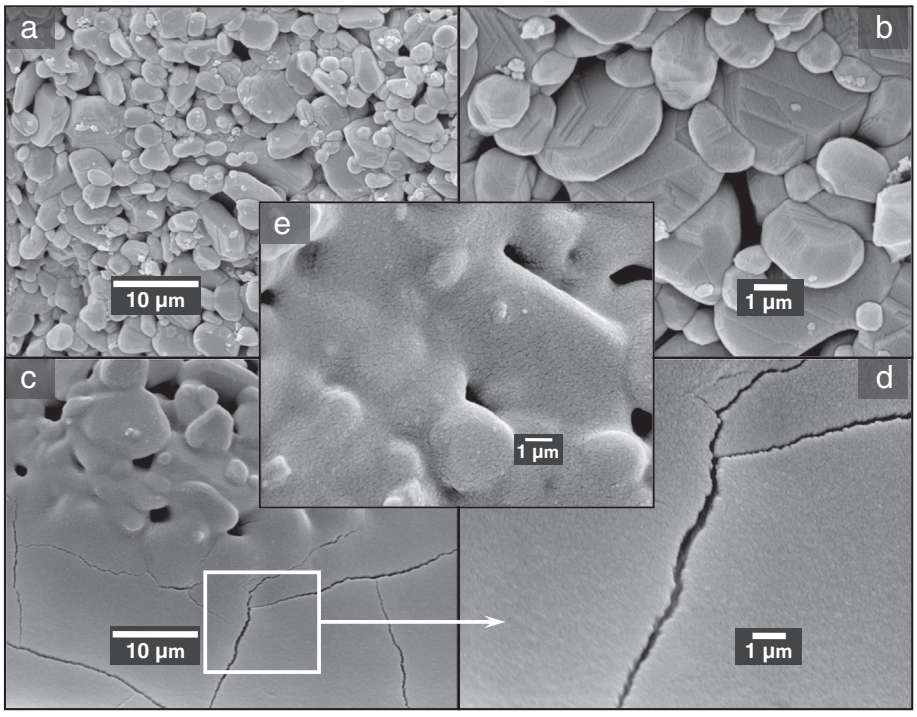

Fig. 4. SEM micrographs of the foam (a, b) and catalytic coating (c, d, e).

main signal of CeO_2 with very low intensity, also suggesting that probably the active phases were formed with a low crystallinity degree and hence the crystallite sizes were about few nanometers.

Fig. 5 shows the Raman spectra of the structured systems. The cerium-free sample presents a broad and asymmetrical band corresponding to the stretching of the Ni–O bond centered at 540 cm^{-1}. The position of this signal, shifted to higher frequencies with respect to that of bulk nickel oxide (500 cm^{-1}), is associated with the strong interaction between the alumina and nickel species. Furthermore, a broad shoulder at ~400 cm^{-1}, assigned to surface vacancies in the material, was visualized together with weak bands at 700 and 1080 cm^{-1} associated with second order phononic modes.

Cerium-containing samples showed the same bands corresponding to the stretching of the Ni–O bond, although this main signal shifted ~15 cm^{-1} towards higher frequencies.

In addition, the spectra of the cerium-promoted systems showed a strong and sharp signal at ~465 cm^{-1}, assigned to the F2g vibration mode, characteristic of CeO_2 with fluorite-type structure. This vibration mode is related to the oxygen atoms surrounding the Ce^{4+} cation. The shift toward lower frequencies (~5–10 cm^{-1}) suggests a change in the parameters of the crystal lattice and the presence of oxygen vacancies. The change in the position of the main band followed a general tendency: catalysts with higher amount of promoter shifted less than those with a lower amount of cerium (Fig. 5 inset).

Moreover, additional sharp bands at 224 cm^{-1} and 632 cm^{-1} both associated with distortions of oxygen network, were clearly observed; thus a modification in the ceria structure was confirmed.

It is possible to estimate the crystallite size of the CeO_2 from the Raman spectra by Graham's equation [21,22]. The sizes were 1.7, 2.5, 2.9 and 5.8 nm for catalysts with Ce/Ni = 0.05, 0.11, 0.17 and 0.25 atomic ratios, respectively, demonstrating that nanometric crystallites were formed in the catalytic layer, in agreement with the XRD results. As expected, the crystalline domain size of the ceria phase grows with the increment in the amount of the promoter.

The XPS spectrum of the Ni – AF sample shows the Ni $2p_{3/2}$ main signal positioned at 855.3 eV with a satellite at 861.5 eV. It was reported that the binding energy (BE) corresponding to Ni $2p_{3/2}$ of bulk NiO was about ~854.0 eV. Consequently, nickel could not be on the surface as free NiO. The higher binding energy is related to Ni^{2+} surface species, with a strong interaction with the support. In addition, a difference between the Ni $2p_{3/2}$ and Ni $2p_{1/2}$ main peaks of about 17.7 eV could be observed. This result is also in agreement with the absence of bulk nickel oxide in the surface since in the case of bulk NiO this difference is around 18.6 eV [23].

Similar results were visualized on the Ni $2p_{3/2}$ spectra of bimetallic oxide catalysts. However, neither signals of Ni $2p_{1/2}$ nor signals of Ce $3d_{5/2}$ in the 870–895 eV region could be properly differentiated since they overlapped. Nevertheless, the region corresponding to the Ce $3d_{3/2}$ level (895–925 eV) displayed signals that suggest a majority of Ce^{4+} species.

3.2.4. Composition and distribution of the active phases

Through the EDX technique, the atomic ratios of the components in the catalytic coatings (Ni, Al, Ce) were quantified. Although numerous foam regions were analyzed, only a summary of the three most representative results is shown in Table 1.

The monometallic oxide system showed a quite homogeneous Ni/Al ratio throughout the structure. This behavior was also observed in cerium-promoted samples. Furthermore, Ce/Ni ratios were close to the nominal values indicating that the active phases were reasonably well spread along the surface. In addition, Ce/Al ratios were similar in most of the studied sectors, also revealing a uniform distribution of these components.

4. Conclusions

Ni and Ni–Ce/alumina catalysts were appropriately deposited onto ceramic foams. They were morphologically uniform and mechanically stable.

The systems showed activity and selectivity for the ODE reaction, demonstrating that the incorporation method was successful to obtain adequate active sites. The component distribution was homogeneous indicating that the impregnation procedure was suitable.

The presence of cerium markedly enhanced the catalytic activity due to a synergistic effect with NiO related to the incorporation of the nickel

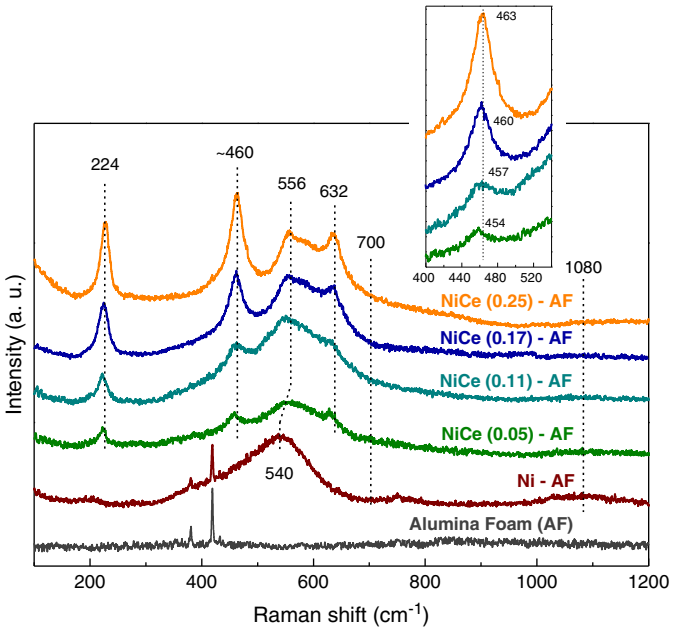

Fig. 5. Laser Raman spectra of the catalysts. Inset: Ceria typical band.

Table 1
EDX results of the components in the coverage.

Catalyst	Atomic ratio		
	Ni/Al	Ce/Ni	Ce/Al
Ni – AF	0.11	–	–
	0.10	–	–
	0.11	–	–
NiCe (0.05) – AF	0.26	0.07	0.02
	0.20	0.06	0.01
	0.20	0.06	0.01
NiCe (0.11) – AF	0.09	0.12	0.01
	0.16	0.12	0.02
	0.15	0.13	0.02
NiCe (0.17) – AF	0.16	0.20	0.02
	0.16	0.20	0.03
	0.21	0.16	0.03
NiCe (0.25) – AF	0.17	0.24	0.02
	0.18	0.23	0.02
	0.16	0.27	0.02

cation into the ceria lattice. However, there is an optimal Ce/Ni ratio that maximizes the catalytic performance.

The ethane conversion was clearly improved in cerium-promoted systems but the selectivity was slightly lower, leading to a significant increment in ethylene productivity compared to the cerium-free system. Therefore, the Ni and Ni–Ce alumina-supported structured systems were efficient for ethene production.

References

[1] J.A. Moulijn, M.T. Kreutzer, T.A. Nijhuis, F. Kapteijn, Adv. Catal. 54 (2011) 249–327.
[2] W. Wei, X.M. Cao, C. Tian, J.S. Zhang, Microporous Mesoporous Mater. 112 (2008) 521–525.
[3] N. Gokon, Y. Osawa, D. Nakazawa, T. Kodama, Int. J. Hydrog. Energy 34 (2009) 1787–1800.
[4] M.A. Ulla, R. Mallada, L.B. Gutierrez, L. Casado, J.P. Bortolozzi, E.E. Miró, J. Santamaría, Catal. Today 133–135 (2008) 42–48.
[5] Q. Liu, Z. Liu, J. Su, Catal. Today 158 (2010) 370–376.
[6] K.S. Yang, Z. Jiang, J.S. Chung, Surf. Coat. Technol. 168 (2003) 103–110.
[7] Y. Li, Y. Li, Q. Yu, L. Yu, Catal. Commun. 29 (2012) 127–131.
[8] L. Giani, G. Groppi, E. Tronconi, Ind. Eng. Chem. Res. 44 (2005) 4993–5002.
[9] L.J. Gibson, M.F. Ashby, Cellular Solids: Structure and Properties, Second edition Cambridge University Press, Cambridge, United Kingdom, 1999.
[10] J.T. Richardson, Y. Peng, D. Remue, Appl. Catal. A Gen. 204 (2000) 19–32.
[11] J.T. Richardson, D. Remue, J.K. Hung, Appl. Catal. A Gen. 250 (2003) 319–329.
[12] M.V. Twigg, J.T. Richardson, Chem. Eng. Res. Des. 80 (2002) 183–189.
[13] M.V. Twigg, J.T. Richardson, Ind. Eng. Chem. Res. 46 (2007) 4166–4177.
[14] A. Löfberg, A. Essakhi, S. Paul, Y. Swesi, M.L. Zanota, V. Meille, I. Pitault, P. Supiot, B. Mutel, V. LeCourtois, E. Bordes–Richard, Chem. Eng. J. 176–177 (2011) 49–56.
[15] E. Heracleous, A.A. Lemonidou, J. Catal. 270 (2010) 67–75.
[16] B. Solsona, P. Concepción, S. Hernández, B. Demicol, J.M. López Nieto, Catal. Today 180 (2012) 51–58.
[17] P. Botella, E. García–González, A. Dejoz, J.M. López Nieto, M.I. Vázquez, J. González–Calbet, J. Catal. 225 (2004) 428–438.
[18] T.T. Nguyen, L. Burel, D.L. Nguyen, C. Pham–Huu, J.M.M. Millet, Appl. Catal. A Gen. 433–434 (2012) 41–48.
[19] A. Essakhi, A. Löfberg, S. Paul, B. Mutel, P. Supiot, V. LeCourtois, P. Rodriguez, V. Meille, E. Bordes–Richard, Microporous Mesoporous Mater. 140 (2011) 81–88.
[20] [20] J.P. Bortolozzi, Doctoral Thesis, UNL, 2013.
[21] G.W. Graham, W.H. Weber, C.R. Peters, R. Usmen, J. Catal. 130 (1991) 310–313.
[22] S. Kanakaraju, S. Mohan, A.K. Sood, Thin Solid Films 305 (1997) 191–195.
[23] E. Heracleous, A.F. Lee, K. Wilson, A.A. Lemonidou, J. Catal. 231 (2005) 159–171.